Research Article

Cancer Immunology Research

PPAR-Induced Fatty Acid Oxidation in T Cells Increases the Number of Tumor-Reactive CD8$^+$ T Cells and Facilitates Anti–PD-1 Therapy

Partha S. Chowdhury, Kenji Chamoto, Alok Kumar, and Tasuku Honjo

Abstract

Although PD-1 blockade cancer immunotherapy has shown potential for a wide range of patients with cancer, its efficacy is limited, in part, due to the loss of effector cytotoxic T lymphocytes (CTLs) via terminal differentiation–induced apoptosis. We previously demonstrated that mitochondrial activation, by the agonists of peroxisome proliferator–activated receptor γ (PPARγ) coactivator 1-α (PGC-1α)/transcription factor complexes, had synergistic effects with a PD-1–blocking monoclonal antibody in a mouse tumor model. In the current study, we examined the molecular mechanism of the synergistic effects of bezafibrate, an agonist of PGC-1α/ PPAR complexes, which enhanced the tumoricidal effects of PD-1 blockade. Bezafibrate activated CTL mitochondria and upregulated oxidative phosphorylation as well as glycolysis, resulting in more proliferation of naïve T cells and improved effector function in CTLs. Bezafibrate also increased fatty acid oxidation (FAO) and mitochondrial respiratory capacity, which supports the extra energy demands of cells in emergencies, allowing cell survival. Carnitine palmitoyl transferase 1 (Cpt1), which is needed for FAO, and Bcl2 were both upregulated. Cpt1 and Bcl2 can form a complex to prevent apoptosis of CTLs. Together, these results indicate that bezafibrate increases or maintains the number of functional CTLs by activating mitochondrial and cellular metabolism, leading in turn to enhanced antitumor immunity during PD-1 blockade. *Cancer Immunol Res; 6(11); 1375–87. ©2018 AACR.*

Introduction

The checkpoint molecules CTLA-4 and PD-1 regulate the balance between immune surveillance by immune cells and immune escape by tumor cells (1–3). Inhibition of CTLA-4 and PD-1 with monoclonal antibodies (mAbs) suppresses tumor growth in animal models (4, 5). Clinical trials using these immune-checkpoint blockade mAbs led to FDA approval of ipilimumab (CTLA-4) and nivolumab (PD-1) for use in cancer treatment (6, 7). Nivolumab demonstrated durable clinical activity with less severe side effects than ipilimumab (8, 9). The FDA has approved additional antibodies such as pembrolizumab and durvalumab against PD-1 or its ligand PD-L1 to treat various human cancers, including melanoma, non–small cell lung carcinoma, kidney cancer, non-Hodgkin lymphoma, head and neck cancer, urothelial carcinoma, hepatocellular carcinoma, and gastric cancer (10).

Although PD-1 blockade therapy shows several advantages compared with conventional chemotherapies, a substantial number of patients do not respond to this therapy (10). Therefore, biomarkers for distinguishing responders from nonresponders before initiating PD-1 blockade treatment and combination therapy to improve PD-1 blockade efficacy must be developed. Despite attempts to identify biomarkers for cancer immunotherapy, only PD-L1 expression was informative for non–small cell lung carcinoma in the clinic (11, 12). To overcome the low response rate of PD-1 blockade therapy, various combinations involving chemotherapies, radiotherapy, cancer vaccines, other immune-checkpoint inhibitors, and several immune-stimulatory agents have been examined (10), but with disappointing results. The FDA has approved only two combinations for PD-1 blockade: CTLA-4 blockade or chemotherapy (13, 14).

Infiltration of lymphocytes to tumor sites is a prognostic factor for numerous cancers (15, 16). Additionally, the efficacy of PD-1 blockade is correlated with the infiltration of CD8$^+$ T cells in tumors (17). Thus, it is necessary to understand the mechanism of tumor-reactive CTL activation and differentiation to control tumoricidal effects during PD-1 blockade. Naïve T cells are converted into effector T cells, which are responsible for tumor clearance, with an increased glycolytic rate during immune responses. After antigen clearance, a small fraction of T cells differentiate into long-surviving memory T cells, whose energy generation depends mainly on fatty acid oxidation/oxidative phosphorylation (FAO/OXPHOS) in the mitochondria (18).

PD-1 blockade enhances glycolysis in T cells and is responsible for recovery of effector function (19). The role of mitochondrial energy metabolism during development of T-cell antitumor immunity mediated by PD-1 blockade, however, remains unclear. Mitochondria are activated in tumor-reactive CTLs during PD-1 blockade therapy, indicating that T-cell activation and differentiation are associated with mitochondrial energy metabolism (20). Less mitochondrial activation was observed in CTLs derived from mice bearing PD-1 blockade–insensitive tumors, suggesting that mitochondrial activation may serve as a biomarker for the effectiveness of PD-1 blockade therapy (20). Others have shown

Department of Immunology and Genomic Medicine, Graduate School of Medicine, Kyoto University, Kyoto, Japan.

Note: Supplementary data for this article are available at Cancer Immunology Research Online (http://cancerimmunolres.aacrjournals.org/).

P.S. Chowdhury and K. Chamoto contributed equally to this article.

Corresponding Author: Tasuku Honjo, Graduate School of Medicine, Kyoto University, Yoshida Konoe-cho, Sakyo-ku, Kyoto 606-8501, Japan. Phone: 81-75-753-4371; Fax: 81-75-753-4388; E-mail: honjo@mfour.med.kyoto-u.ac.jp

doi: 10.1158/2326-6066.CIR-18-0095

that PGC-1α, a regulator of mitochondrial biogenesis, is important for development of T-cell–mediated antitumor immunity (21). We demonstrated previously that activation of PGC-1α/peroxisome proliferator–activated receptors (PPAR) by bezafibrate improves the efficacy of PD-1 blockade (20). However, the mechanism by which the PPAR pathway activates antitumor immunity remains unknown.

In this study, we investigated the effect of bezafibrate on the phenotype of effector $CD8^+$ T cells and on mitochondria. We investigated the molecular mechanism by which bezafibrate modulates CTL differentiation and enhances T-cell–based antitumor immunity. We found that bezafibrate promotes differentiation of naïve to effector T cells, upregulates FAO, and inhibits apoptosis of effector T cells. These different effects of bezafibrate on the priming and effector phases resulted in increased numbers of functional effector T cells and improved effectiveness of PD-1 blockade. Therefore, combining the reprogramming of energy metabolism through PPAR signaling in T cells with PD-1 blockade may be a promising strategy for combination therapy.

Materials and Methods

Mice and cells

C57BL/6N and BALB/c mice were purchased from The Charles River Laboratory. $CD8^{-/-}$ mice were provided from The Jackson Laboratory (originally from Univ. Toronto, T.W. Mak). Mice were approximately 5 to 6 weeks old at the time of the experiment and maintained under specific pathogen-free conditions at the Institute of Laboratory Animals, Graduate School of Medicine, Kyoto University, under the direction of the institutional review board. The murine fibrosarcoma cell line (MethA) was obtained from the Cell Resource Center for Biomedical Research, and murine colon carcinoma cell line (MC38) was a gift from Dr. James P. Allison, Memorial Sloan-Kettering Cancer Center (New York, NY). Cell lines were cultured in RPMI medium (Gibco; 11875-093) with 10% (v/v) heat-inactivated fetal bovine serum and 1% (v/v) penicillin–streptomycin mixed solution (Nacalai Tesque; 26253-84). Cell lines were free of *mycoplasma* contamination. Cell lines were used within fifth passage and were not authenticated in the past year.

Mouse therapy model

A total of 5×10^5 cells of MC38 and MethA were intradermally (i.d.) injected into the right flank of C57BL/6N and BLAB/c mice, respectively (day 0). Combination therapy was started when the tumor size reached 60 to 70 mm^3 (around day 7). Mice were intraperitoneally (i.p.) injected with 40 μg of anti–PD-L1 (clone 1-111A.4) and mAb injection was repeated every sixth day. Bezafibrate (Santa Cruz Biotechnology) was i.p. injected at 2.5 mg/kg every third day. For untreated mice, an isotype control for anti–PD-L1 (Rat IgG2a) was injected. Tumor measurement was performed on each alternate day and tumor volume was calculated using the formula for typical ellipsoid $\pi \times$ (length $\times$ breadth $\times$ height)/6.

$CD8^{-/-}$ mouse model

$CD8^+$ T cells were isolated from the lymph node and spleen of CD45.1 congenic mice using an autoMACS Pro Separator (Miltenyi Biotec). After washing with PBS, $CD8^+$ T cells were labeled with CellTrace Violet (Thermo Fisher Scientific). For labeling, $CD8^+$ T cells were incubated for 15 minutes with CellTrace diluted in PBS. After quenching with complete media and washing the cells twice with PBS, the labeled $CD8^+$ $CD45.1^+$ T cells were intravenously (i.v.) injected in to CD45.2 $CD8^{-/-}$ mice. MC38 cells (5×10^5 cells) were i.d. injected 2 days after $CD8^+$ T-cell infusion. Anti–PD-L1 and bezafibrate were i.p. administered 5 days after tumor inoculation. Mice were sacrificed on day 9 for analysis.

Chemical reagents

Bezafibrate was used at the dose of 2.5 mg/kg for combination therapy. Bezafibrate was freshly prepared immediately before use in DMSO. Dissolved bezafibrate was diluted in PBS and 200 μL was i.p. injected per mouse. Bezafibrate was added at the concentration of 30 μmol/L for the entire culture period.

Naïve $CD8^+$ T-cell sorting using AutoMACS

To isolate naïve $CD8^+$ T cells from C57BL/6N wild-type mice, the spleen and three LNs (axillary, brachial, and inguinal LNs) from both the right and left sides were harvested. The spleen was minced, treated with ACK buffer for 2 minutes to lyse erythrocytes, and mixed with pooled and minced LN cells. Naïve ($CD44^-$) $CD8^+$ T cells were then purified from total pooled lymphocytes according to the manufacturer's instructions (Miltenyi Biotec; 130-096-543).

Cell preparation for analysis

For draining lymph node (DLN) analysis, axillary, brachial, and inguinal LNs (one of each) were harvested from the right side of tumor-bearing mice. All LNs were minced and pooled. Average LN cell numbers (total pooled LN cells/3) were used as absolute cell numbers. For tumor-infiltrating lymphocyte (TIL) analysis, tumor tissue was harvested and minced into 1- to 2-mm pieces with scissors followed by digestion with collagenase type IV (Worthington Biochemical Corporation) using a gentleMACS Dissociator (Miltenyi Biotec). The numbers of TILs per mg of tumor tissue were used as the absolute numbers. For *in vitro* analysis, naïve $CD8^+$ T cells were stimulated with beads coated with anti-CD3 and CD28 (Thermo Fisher Scientific) and with recombinant human IL2 (100 U/mL; PeproTech). The expanded T cells on days 2 and 13 were used for proliferation assays and apoptosis assays, respectively.

Flow cytometry analysis

The following monoclonal antibodies (mAb) were used to detect the respective antigens: CD44 (IM7), CD45.2 (104), CD45.1 (A20), CD8 (53-6.7), CD62L (MEL-14), T-bet (4B10), IFNγ (XMG-1.2), and Bcl-2 (BCL/10C4) from BioLegend; EOMES (Dan11mag), and Ki67 (SolA15) from eBioscience: Cpt1a (8F6AE9) from Abcam. All flow cytometry experiments were performed on a FACSCanto II (BD Biosciences) and analyzed using FlowJo software (FlowJo, LLC). Details of intracellular staining were mentioned previously (20). Mitochondrial mass, mitochondrial potential, mitochondrial superoxide, and cellular reactive oxygen species (ROS) were determined by MitoTracker Green, MitoTracker Deep Red, MitoSOX Red, and CellROX Green reagents, respectively (all from Life Technologies). These dyes were added to the cells at final concentrations of 0.125, 0.125, 5.0, and 0.625 μmol/L and incubated at 37°C in a 5% CO_2 humidified incubator for 30 minutes, followed by surface staining.

Measurement of oxygen consumption rates and extracellular acidification rate

Oxygen consumption rate (OCR) and extracellular acidification rate (ECAR) of $CD8^+$ T cells isolated from treated mice were measured using an XF^e96 Extracellular Flux analyzer (Seahorse Biosciences). Cells (400,000 per well) were seeded in an XF^e96 plate, determined by titration, as previously described (20). Different parameters from the OCR graph were calculated. ATP turnover was defined as follows: (last rate measurement before oligomycin) − (minimum rate measurement after oligomycin injection). Maximal respiration was defined as follows: (maximum rate measurement after FCCP) − (nonmitochondrial respiration). Spare respiratory capacity (SRC) was calculated by subtracting basal respiration from maximal respiration. We measured the ECAR value in the same well, which contained an optimal glucose level so the basal ECAR (or glycolysis) value is the reading we obtained immediately before oligomycin injection. We prepared the assay medium as described in the XF cell Mito Stress Test Kit (Kit 103015-100). The glucose concentration in this medium is 10 mmol/L. In the classic glycolytic assay procedure (glucose-free media), the final concentration of glucose added to the port is 10 mmol/L while measuring flux. The basal ECAR value in this method is calculated by subtracting the last rate measurement before glucose injection from the maximum rate measurement before oligomycin injection, which gives the same value as calculated by our method. Glycolytic capacity was defined as the rate measured after oligomycin injection. Glycolytic reserve was defined as follows: (glycolytic capacity) – (basal ECAR value) (22).

Real-time RT-PCR

We isolated RNA from purified $CD8^+$ T cells with the RNeasy mini kit (QIAGEN) and synthesized cDNA by reverse transcription (Invitrogen). The primers used to perform real-time PCR are listed in Supplementary Table S1.

Microarray analysis

Total RNA was extracted using the RNeasy Micro kit (QIAGEN) according to the manufacturer's protocols. $CD8^+$ T cells expanded *in vitro* until day 13 were lysed according to the protocol. Microarray analysis was performed by Macrogen using GeneChip Mouse Gene 2.0 ST Array. The data were deposited at GEO repository (http://www.ncbi.nlm.nih.gov/geo) and the accession number is GSE118659. Gene-enrichment and functional annotation analysis was performed using Gene Ontology (www.geneontology.org/) and KEGG (www.genome.jp/kegg/). All data analysis and visualization of differentially expressed genes was conducted using R 3.1.2 (www.r-project.org).

Western blotting

$CD8^+$ T cells were isolated from DLNs using mouse CD8 MicroBeads (Miltenyi Biotec). After washing the cells with PBS twice, 2×10^6 cells were used. Details were as described (20). Antibodies recognizing p-CREB (ab32096) and Cpt1a (ab128568) were obtained from Abcam.

Statistical analysis

Statistical analysis was performed using Prism 6 (GraphPad Software). One-way ANOVA analysis followed by Sidak multiple comparison test was utilized to analyze three or more variables. To compare two groups, Student *t* test was used. All statistical tests were two-sided assuming parametric data, and a P of <0.05 was considered significant. The variations of data were evaluated as the means ± standard error of the mean (SEM). Five or more samples were thought to be appropriate for the sample size estimate in this study. Samples and animals were randomly chosen from the pool and treated. Treatment of samples and animals was performed unblinded.

Results

Bezafibrate expands $CD8^+$ T cells and enhances effector function of CTLs

In our previous study, we demonstrated mitochondrial activation during PD-1 blockade therapy and developed several combination therapies using mitochondria-activating chemicals. We found that activation of the PGC-1α/PPARs axis by bezafibrate improved the efficacy of PD-1 blockade in murine colon carcinoma (MC38)-bearing C57BL/6 mice (20). We confirmed similar synergistic effects of bezafibrate with anti–PD-L1 on the growth of MethA tumors, a murine skin sarcoma line on a different genetic background, BALB/c (Supplementary Fig. S1A). Bezafibrate treatment alone did not exhibit any antitumor activity, indicating that enhanced antitumor activity is mediated through activated lymphocytes, but not directly through tumor cells (ref. 20; Supplementary Fig. S1B). These results indicate that the combination of bezafibrate with PD-1 blockade is applicable to multiple tumors on different genetic backgrounds.

Because the number of effector killer T cells determines the effect against cancer cells *in vivo*, we first investigated the effect of bezafibrate on the effector phenotype of $CD8^+$ T cells (15–17). Both the frequency and number of effector/memory $CD8^+$ T cells ($CD62L^-$ $CD44^+$ $CD8^+$ T cells, P3) in DLNs were significantly increased by treatment combining anti–PD-L1 and bezafibrate compared with treatment with anti–PD-L1 alone (Fig. 1A). In contrast, the numbers of naïve ($CD62L^+$ $CD44^-$ $CD8^+$ T cells, P1) and central memory T cells ($CD62L^+$ $CD44^+$ $CD8^+$ T cells, P2) were not changed by bezafibrate addition, whereas injection of anti–PD-L1 alone was accompanied by increased P1 and P2 populations (Fig. 1A). Accordingly, $CD8^+$ TILs, which mainly comprise the effector/memory T-cell population (P3), were expanded, as we previously described (ref. 20; Fig. 1B).

We attribute the antitumor effect not only to the number of effector T cells but also to their function. The T-bet/Eomes balance is a factor regulating cytokine synthesis and T-cell differentiation (22). We found that bezafibrate addition increased the amount of T-bet in DLN $CD8^+$ T cells (Fig. 1C). In contrast, the frequency and number of $Eomes^+$ $CD8^+$ T cells decreased or were unchanged after bezafibrate addition (Fig. 1C). These data demonstrate that the bezafibrate enhanced the effector function of CTLs. We further investigated T-bet and Eomes expression in each P1-P3 population. Among subsets of T cells, the P3 population has the most T-bet and the least Eomes; T-bet increased after bezafibrate treatment only in P3 (Supplementary Fig. S2A). Although the naïve population (P1) is present most abundantly in $CD8^+$ T cells, T-bet expression is lowest in this population and is unaffected by bezafibrate treatment (Supplementary Fig. S2A). Bezafibrate combination therapy increased the number of cells only in the P3 population (Fig. 1A). These results suggest that most of the changes in T-bet amounts are due to the P3 population in DLN $CD8^+$ T cells (Fig. 1C). $CD8^+$ TILs are $T\text{-bet}^+$ and $Eomes^-$

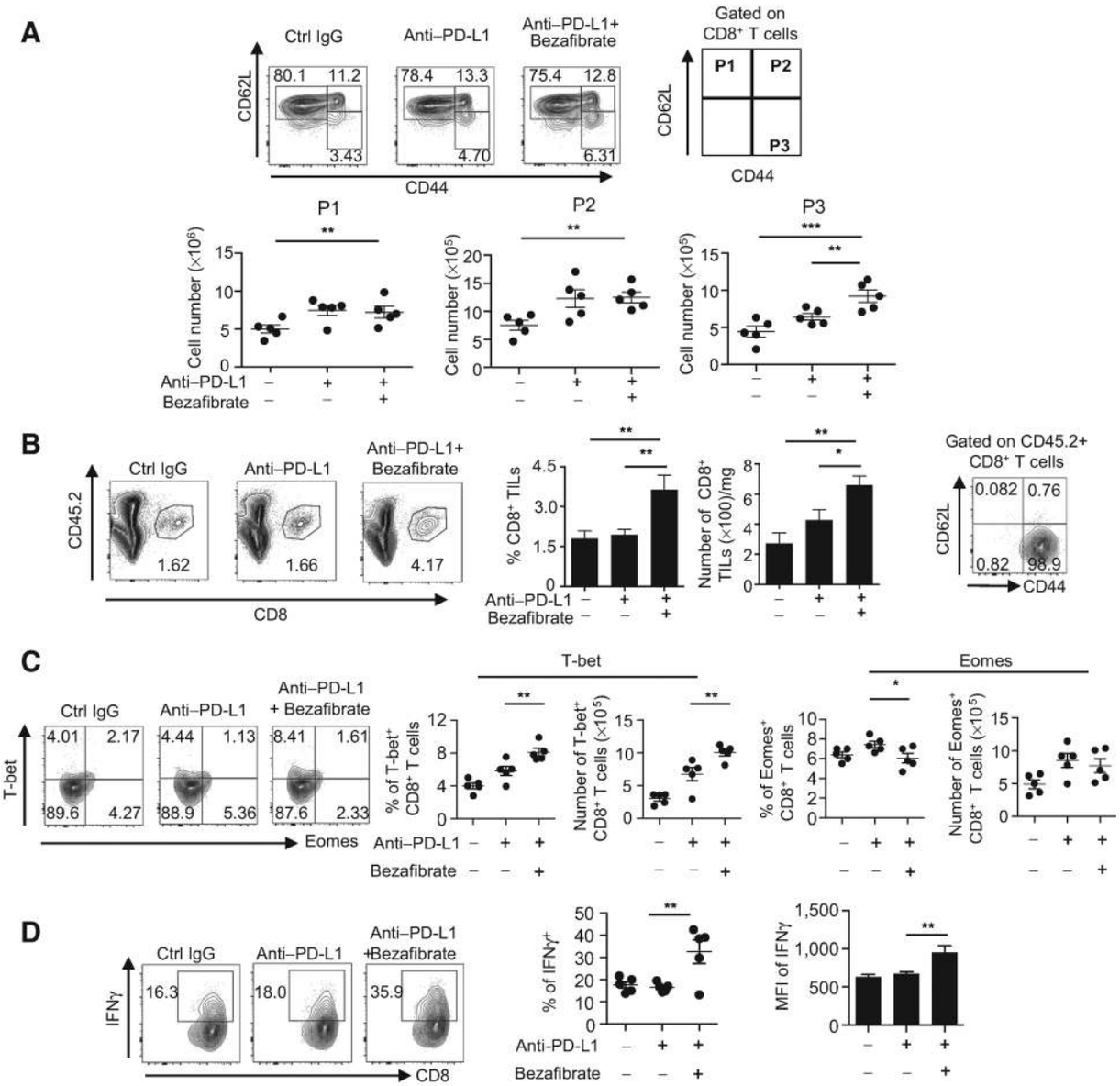

Figure 1.

Bezafibrate improves the quality and quantity of effector CD8$^+$ T cells *in vivo*. MC38-bearing mice were treated with anti–PD-L1 and bezafibrate on the same schedule as shown in Supplementary Fig. S1A. Mice were sacrificed, and CD8$^+$ T cells in DLN and tumor sites were analyzed on the indicated day. **A,** DLN cells on day 15 were stained with anti-CD8, anti-CD62L, and anti-CD44. Representative FACS patterns are shown (top). The absolute numbers of P1–P3 population per one LN were calculated (bottom). **B,** Cells isolated from the tumor mass on day 11 were stained with anti-CD8, anti-CD45.2, anti-CD62L, and anti-CD44. CD45.2$^+$ CD8$^+$ T cells were gated, and representative FACS patterns are shown (left). The frequencies and number of CD45.2$^+$ CD8$^+$ TILs were compared between treated groups (middle). CD62L and CD44 phenotypes after gating at CD45.2$^+$ CD8$^+$ T cells were analyzed (right). **C,** T-bet and Eomes expression was analyzed by flow cytometry in DLN CD8$^+$ T cells on day 15 from treated mice. Representative FACS data are shown (left). The frequency and numbers of T-bet$^+$ or Eomes$^+$ T cells were calculated in DLN CD8$^+$ T cells from treated mice (right). **D,** Digested tumor tissues on day 15 were incubated at 37°C for 6 hours, and IFNγ was intracellularly stained in CD8$^+$ T cells from treated mice. Representative FACS data of CD8$^+$ T cells gated (left), frequency (middle), and MFI (right) of IFNγ$^+$ T cells among CD8$^+$ T cells are shown. **A**–**D**, Data represent the means ± SEM of five mice. Data are representative of two independent experiments. *, $P < 0.05$; **, $P < 0.01$, one-way ANOVA analysis.

(Supplementary Fig. S2B) and exclusively comprised of P3 population (Fig. 1B). These data suggest that bezafibrate treatment enhances the function of effector/memory CD8$^+$ T cells. Indeed, IFNγ in both CD8$^+$ T cells of DLN and CD8$^+$ TILs was upregulated (Supplementary Fig. S2C; Fig. 1D). Together, we showed the bezafibrate combination therapy increases the number and enhances the function of effector/memory CD8$^+$ T cells in DLNs and at the tumor site.

Bezafibrate with PD-1 blockade induces mitochondrial activation in CD8$^+$ T cells

To understand how bezafibrate enhances T-cell–mediated antitumor immunity under PD-1 blockade conditions, we investigated mitochondrial activities in CTLs isolated from DLNs of MC38 tumor-bearing mice treated with bezafibrate and anti–PD-L1. We found that the OCR, an indicator of mitochondrial respiration including basal respiration, as well as maximal respiration and ATP turnover were all significantly higher in CD8$^+$ T cells isolated from DLNs of bezafibrate- and anti–PD-L1-treated mice (Fig. 2A, left; Supplementary Fig. S3A–S3B). SRC, which is calculated by subtracting basal respiration from maximal respiration, of CD8$^+$ T cells isolated from DLNs was significantly higher in the combination-therapy group than after PD-1 blockade alone (Fig. 2A, right). Because SRC has been linked to cell survival, enhancement of SRC by bezafibrate and anti–PD-L1 combination therapy suggests that CD8$^+$ T cells can survive longer (23). We also determined the effect of bezafibrate treatment on the ECAR to measure glycolysis. We observed that the ECAR values in the bezafibrate and anti–PD-L1 combination-therapy group were significantly higher than those in the group treated with anti–PD-L1 alone (Fig. 2B). The higher values for both OCR and ECAR indicated that CTLs were in a metabolically higher state in the bezafibrate combination group (Fig. 2B). The ratio of OCR and ECAR was higher in the bezafibrate combination group than in the group treated with PD-1 blockade alone (Fig. 2C), indicating that bezafibrate combination therapy raised CD8$^+$ T cells to a higher energy state through mechanisms that relied more on mitochondrial metabolism than on glycolysis. Similar results were observed when the mice were sacrificed at a different time point (Supplementary Fig. S3C and S3D).

As the bezafibrate and PD-1 blockade combination enhanced the OCR values compared with PD-1 blockade alone, we investigated the effect of this combination on other mitochondrial activation parameters. The effector/memory population of CD8$^+$ T cells (P3) in any treatment group showed larger mitochondrial areas, higher intensity of MitoTracker DeepRed, and more ROS than either the naïve (P1) or central memory (P2) CD8$^+$ T cells (Fig. 2D and E). Cellular levels of the MitoTracker DeepRed and ROS increased when cells were treated with bezafibrate combined with anti–PD-L1 (Fig. 2E). Similar results were obtained from CD8$^+$ TILs (Fig. 2F). PD-1 blockade significantly reduced various mitochondrial activation parameters in the P3 population as well as in TIL compared with untreated cells (Fig. 2E and F). This reduction may reflect the change of dependency on the energy metabolic pathways from OXPHOS to glycolysis by PD-1 blockade. Indeed, monotherapy enhanced glycolysis-dependent energy production more than OXPHOS (Fig. 2B and C) and (19, 24). In total, bezafibrate and PD-1 blockade combination treatment activated mitochondria in CTLs and increased mitochondrial SRC, contributing to the enhanced survival of CTLs in this group.

Combination therapy enhances mitochondrial biogenesis and FAO in T cells

Because combined bezafibrate and anti–PD-L1 treatment enhanced mitochondrial activities in CD8$^+$ T cells in MC38 tumor-bearing mice, we used qPCR analysis to ask whether the combination therapy affected transcription of genes involved in mitochondrial biogenesis. We detected increased transcription of PGC-1α and transcription factor A–mitochondrial (*TFAM*), both of which regulate mitochondrial biogenesis. Transcription of other mitochondria-associated genes such as Ubiquinol-Cytochrome C Reductase Core Protein I (*Uqcrc1*), NADH:ubiquinone oxidoreductase core subunit S8 (*NDUSF8*), and ATP synthase F1 subunit alpha (*ATP5a1*) also increased in CD8$^+$ T cells from DLNs of mice treated with the combined bezafibrate and PD-1 blockade (ref. 25; Fig. 3A). Because PPAR signaling also activates the FAO pathway, we assessed transcription of enzymes involved in FAO (26). As shown in Fig. 3B, the expression of carnitine palmitoyl transferase 1B (*Cpt1b*), acyl-CoA dehydrogenase long chain (*LCAD*), and acyl-CoA dehydrogenase medium chain (*MCAD*) was significantly increased in CD8$^+$ T cells isolated from DLNs after the combination treatment compared with cells treated with PD-1 blockade alone. We observed that expression of the Cpt1a protein, another FAO enzyme, was increased significantly by bezafibrate combination treatment in CD8$^+$ T cells of both DLN and TIL (Supplementary Fig. S4A and B). Thus, the bezafibrate and PD-1 blockade combination activates mitochondrial biogenesis and FAO in CD8$^+$ T cells *in vivo*.

Combination therapy enhances survival and proliferation of tumor-reactive CTLs

To investigate the effect of combination therapy on tumor-reactive CTLs, we followed our previous strategy to identify the tumor-reactive CTLs in a mouse tumor model (20). Accordingly, CellTrace-labeled CD45.1$^+$ CD8$^+$ T cells were transferred into CD45.2$^+$ CD8$^{-/-}$ mice, and their proliferation in DLNs and tumor sites was examined (Fig. 4A). As tumors grow faster in CD8$^{-/-}$ mice than in wild-type mice, tumor reached to the desired volume for start of the therapy earlier (on day 5) in CD8$^{-/-}$ mice than in wild-type mice (on day 7). Among the transferred CD45.1$^+$ CD8$^+$ T cells, we identified the proliferating cell population as tumor-reactive cells in mice bearing MC38 tumor cells (Fig. 4B). The frequency and number of proliferating CD45.1$^+$ CD8$^+$ T cells were significantly increased in DLNs and at tumor sites of tumor-bearing mice treated with bezafibrate and anti–PD-L1 compared with mice injected with anti–PD-L1 alone (Fig. 4B). The bezafibrate and anti–PD-L1 combination therapy enhanced mitochondrial mass, MitoTracker DeepRed, mitochondrial ROS, and cellular ROS in tumor-reactive CTLs of DLN (Supplementary Fig. S5A).

An increased number of tumor-reactive CTLs enhances antitumor activity in PD-1 blockade therapy, as most PD-1–blocked CTLs undergo terminal differentiation and apoptosis (27). The increase in the number of tumor-reactive CTLs driven by bezafibrate treatment may be caused in two ways: (1) bezafibrate inhibited terminal differentiation and apoptosis of effector T cells or (ii) bezafibrate promoted proliferation associated with the transition from naïve to effector T cells. To test the first possibility, we analyzed apoptotic effector T cells in tumor-reactive CTLs by costaining with annexin V and propidium iodide (PI). We found that combination therapy significantly reduced the percentage of apoptotic cells (annexin V$^+$ PI$^+$ cells) in tumor-reactive CTLs compared with therapy with anti–PD-L1 alone, indicating that bezafibrate addition enhanced survival of tumor-reactive CTLs (Fig. 4C). We also used annexin V and PI staining to analyze the non–tumor-reactive cell population (CellTrace^{high}CD8$^+$ T cells), which includes more live cells than found among the tumor-reactive population (Supplementary Fig. S5B). These observations are consistent with previous reports that showed that upon PD-1 blockade, dysfunctional effector cells regain effector function but die by terminal differentiation (27). We found that the

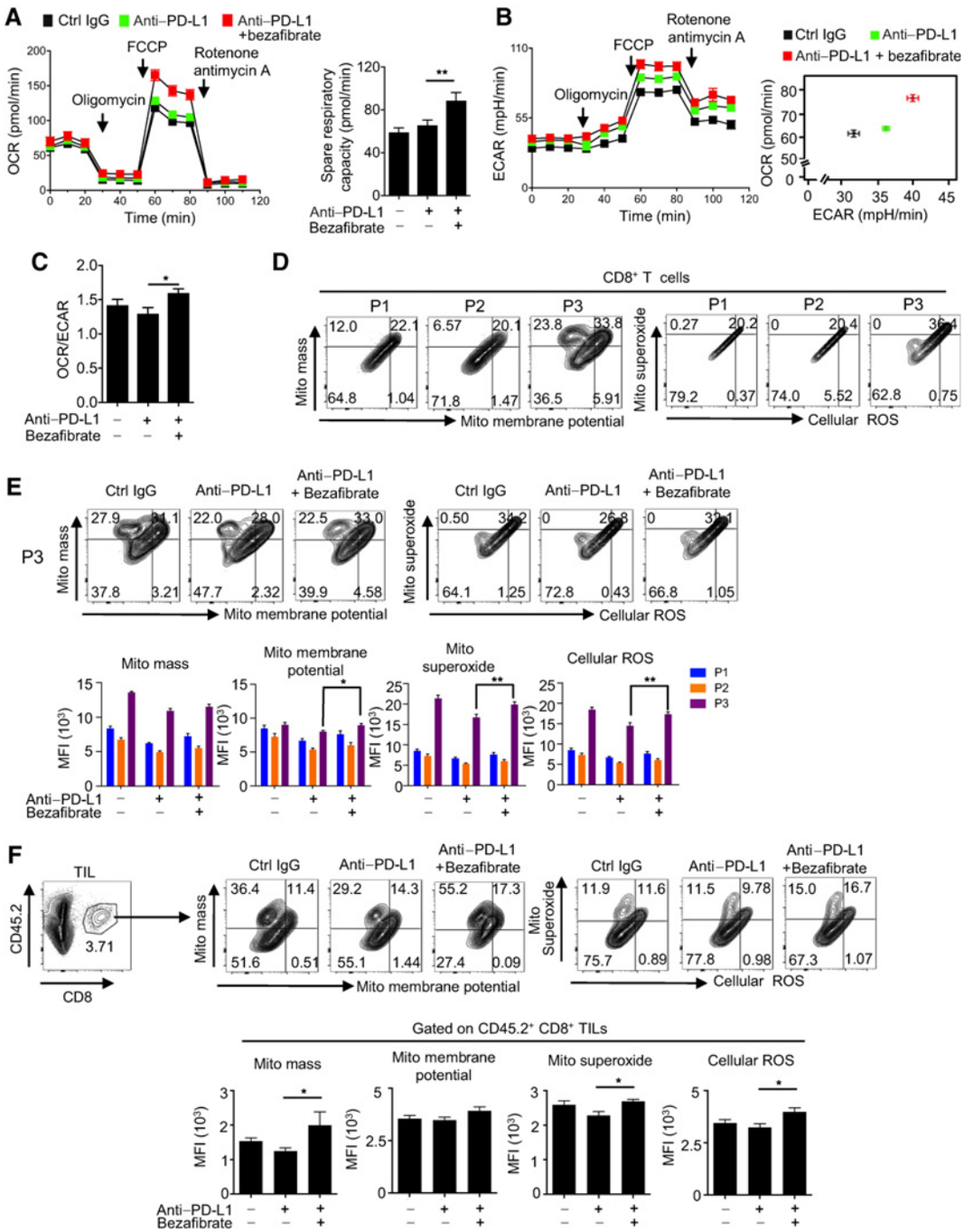

Figure 2.

Bezafibrate combination therapy enhances activation of mitochondria in killer T cells. MC38-bearing mice were treated with anti–PD-L1 and bezafibrate on the same schedule as shown in Supplementary Fig. S1A. On day 9, the mice were sacrificed and $CD8^+$ T cells in DLN and tumor sites were analyzed. **A,** OCR of DLN $CD8^+$ T cells isolated from each group was measured. Cells were pooled from five mice. SRC were calculated. **B,** ECAR of the same cells used in **A** was measured and basal ECAR was calculated. Basal OCR and ECAR values from all treated groups are plotted. **C,** OCR/ECAR ratio was measured. **D,** DLN cells were stained with anti-CD8, anti-CD62L, and anti-CD44. Representative FACS profiles of P1–P3 stained with the indicated mitochondrial dyes in the mice treated with anti–PD-L1 and bezafibrate are shown. **E,** Representative FACS profiles of P3 population stained with the indicated mitochondrial dyes in each group are shown (top). MFI of P1–P3 stained with each dye was compared between treated groups (bottom). Colors correspond to those of the P1–P3 populations. **F,** Cells isolated from the tumor mass were stained with anti-CD8 and anti-CD45.2. $CD45.2^+$ $CD8^+$ T cells were gated (top left). Representative FACS profiles of $CD45.2^+$ $CD8^+$ T cells stained with each mitochondrial dye in mice treated with anti–PD-L1 and bezafibrate (top right). MFI of $CD45.2^+$ $CD8^+$ T cells stained with each dye were compared between treated groups (bottom). **A–C**, Data represent the means ± SEM of 6 wells. Data are representative of two independent experiments. *, $P < 0.05$; **, $P < 0.01$, one-way ANOVA analysis. **E–F**, Data represent the means ± SEM of 5 mice. Data are representative of two independent experiments. *, $P < 0.05$; **, $P < 0.01$, one-way ANOVA analysis.

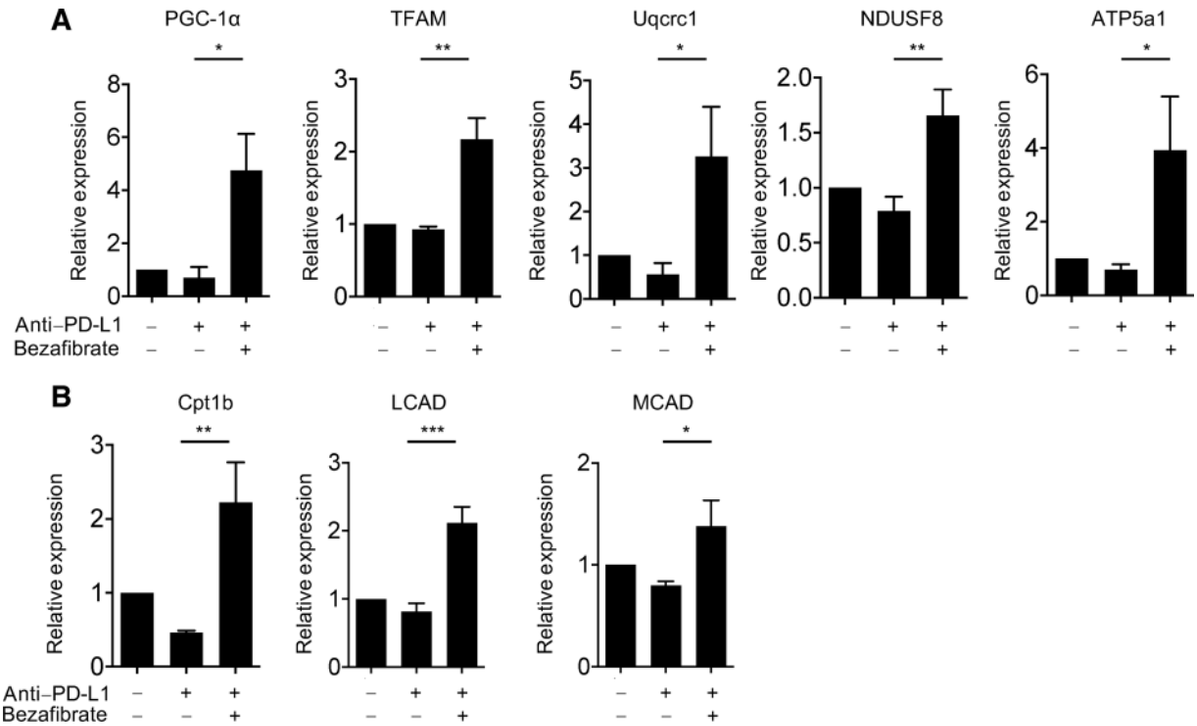

Figure 3.

Bezafibrate combination therapy enhances expression of genes associated with mitochondrial biogenesis and FAO in CD8$^+$ T cells *in vivo*. **A** and **B,** MC38-bearing mice were treated with anti–PD-L1 and bezafibrate on the same schedule as shown in Supplementary Fig. S1A. Mice were sacrificed on day 9, and CD8$^+$ T cells isolated from DLN were pooled from 5 mice. *PGC-1α*, *TFAM*, *Uqcrc1*, *NDUSF8*, *ATP5a1*, *Cpt1b*, *LCAD*, and *MCAD* expression was examined by quantitative PCR (qPCR) in DLN CD8$^+$ T cells of treated groups. Data represent the means ± SEM of 3 wells assuming the untreated group = 1 in qPCR analysis. Expression in each group was compared with the anti-PD-L1 treated group. *, $P < 0.05$; **, $P < 0.01$; ***, $P < 0.001$, one-way ANOVA analysis.

bezafibrate combination treatment significantly increased expression of the antiapoptotic factor, Bcl2, in tumor-reactive CTLs at tumor sites (Fig. 4D).

Next, we investigated the second possibility by determining the expression of Ki67, a marker of cell proliferation, in CD8$^+$ T cells of DLNs (Fig. 4E). We found that the number of Ki67$^+$ CD8$^+$ T cells increased significantly after bezafibrate combination therapy (Fig. 4E). The Ki67$^+$ CD8$^+$ T-cell number was increased in both P3 and P2 populations by the bezafibrate combination therapy (Fig. 4E). Together, these data suggest that the bezafibrate and PD-1 blockade in combination increased the number of tumor-reactive CTLs in DLN and at the tumor site by enhancing their survival capacity and proliferation.

Bezafibrate improves survival capacity of *in vitro*–stimulated CTLs

To analyze the mechanism by which PPAR signaling inhibits apoptosis, we investigated the effect of bezafibrate on the survival capacity of CD8$^+$ T cells *in vitro*. Naïve CD8$^+$ T cells were stimulated as shown in Fig. 5A and expanded until day 13 in the presence of bezafibrate or solvent (DMSO) control. The effect of bezafibrate on T-cell longevity was tested in an over-activation-induced cell death system. After restimulation with anti-CD3 and anti-CD28 on day 13, bezafibrate treatment significantly reduced the number of apoptotic cells (Fig. 5B). Basal OCR and ECAR were not changed by bezafibrate treatment on day 13, but SRC and the OCR/ECAR ratio were significantly increased in the bezafibrate-treated group, again indicating that bezafibrate increased the survival capacity of CTLs (Fig. 5C). We confirmed that bezafibrate significantly increased the expression of *Bcl2*, *Birc3*, and *API5* genes involved in the apoptosis inhibition pathway (Fig. 5D). We further performed GeneChip analysis to identify or differentiate gene-expression signatures between solvent control and bezafibrate-treated CD8$^+$ T cells on day 13 (Supplementary Fig. S6A and S6B). KEGG pathway analysis demonstrated that bezafibrate-treated cells on day 13 displayed differential changes among genes involved in various pathways such as PPAR signaling, fatty acid metabolism, AMPK signaling, cytokine–cytokine receptor interaction, chemokine signaling pathway, complement and coagulation cascades, natural killer cell–mediated toxicity, and metabolism (Supplementary Fig. S6C and S6D).

We focused on upregulated genes involved in preventing apoptosis and analyzed the protein interactome using the STRING database. We found that Bcl2 may be stabilized by interacting with Cpt1, which is also induced by PPAR signaling (ref. 28; Fig. 5E). PPAR regulates cyclic AMP response element binding (CREB), which enhances the expression of PGC-1α in a feed-forward way (refs. 29–32; Fig. 5E). Indeed, both protein and mRNA of Cpt1a and CREB1 were upregulated in bezafibrate-treated CD8$^+$ T cells on day 13 (Fig. 5F and G).

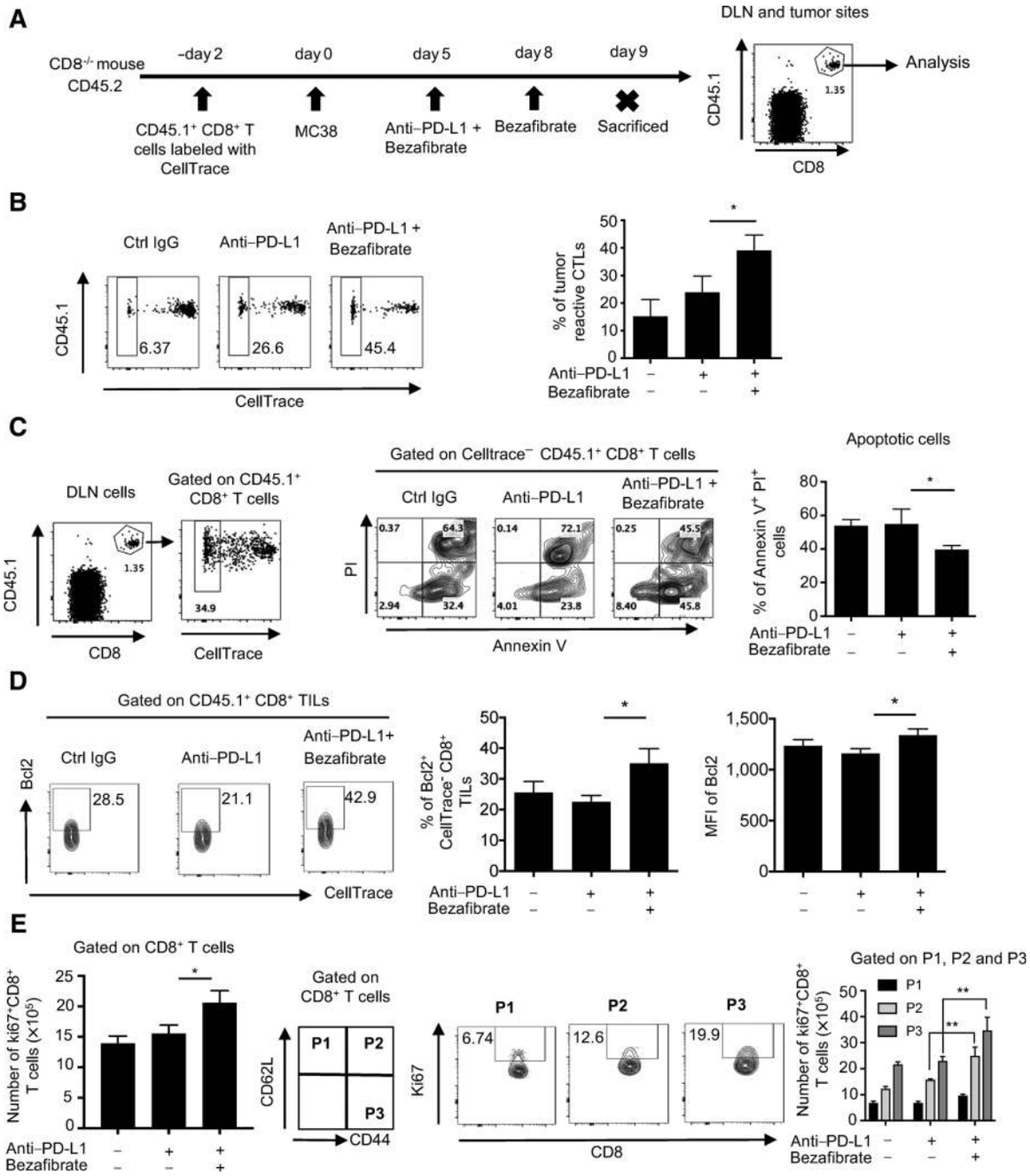

Figure 4.

Bezafibrate increases the number of effector CTLs by enhancing their survival capacity and proliferation. **A–D,** CellTrace-labeled CD45.1$^+$ CD8$^+$ T cells were transferred into CD45.2$^+$ CD8$^{-/-}$ mice. The mice were inoculated with MC38 and treatment started 5 days after MC38 inoculation. Mice were sacrificed on day 9, and CD8$^+$ CD45.1$^+$ T cells in DLNs and tumor sites were analyzed. **A,** A schematic diagram of the experimental schedule. **B,** Representative FACS patterns stained with CD45.1 and CellTrace among the gate of CD8$^+$ CD45.1$^+$ T cells are shown (left). The frequencies of fully proliferated cells (tumor-reactive CTLs) were compared between groups (right). **C,** DLNs were stained with annexin V and propidium iodide (PI). Representative FACS profiles of annexin V and PI staining after gating on CellTrace$^-$ CD45.1$^+$ CD8$^+$ T cells are shown (left and middle). Frequency of apoptotic cells (annexin V$^+$ PI$^+$) was compared between treated groups (right). **D,** CD8$^+$ CD45.1$^+$ T cells in TILs were intracellularly stained with Bcl2. Representative FACS profiles of Bcl2 staining are shown (left). Frequency and MFI of Bcl2$^+$ T cells among CD8$^+$ T cells are shown (right). **E,** MC38-bearing mice were treated with anti–PD-L1 and bezafibrate on the same schedule as shown in Supplementary Fig. S1A. DLN cells on day 13 were stained with anti-CD8, anti-CD62L, anti-CD44, and Ki67. The number of Ki67$^+$ T cells in CD8$^+$ T cells is shown (left). Representative FACS profiles of P1–P3 among CD8$^+$ T cells stained with Ki67 in mice treated with anti–PD-L1 and bezafibrate (middle). The number of Ki67$^+$ T cells in P1–P3 was compared between treated groups. Colors correspond to the P1–P3 populations (right). **B–E,** Data represent the means ± SEM of four or five mice. Data are representative of two independent experiments. *, $P < 0.05$; **, $P < 0.01$, one-way ANOVA analysis.

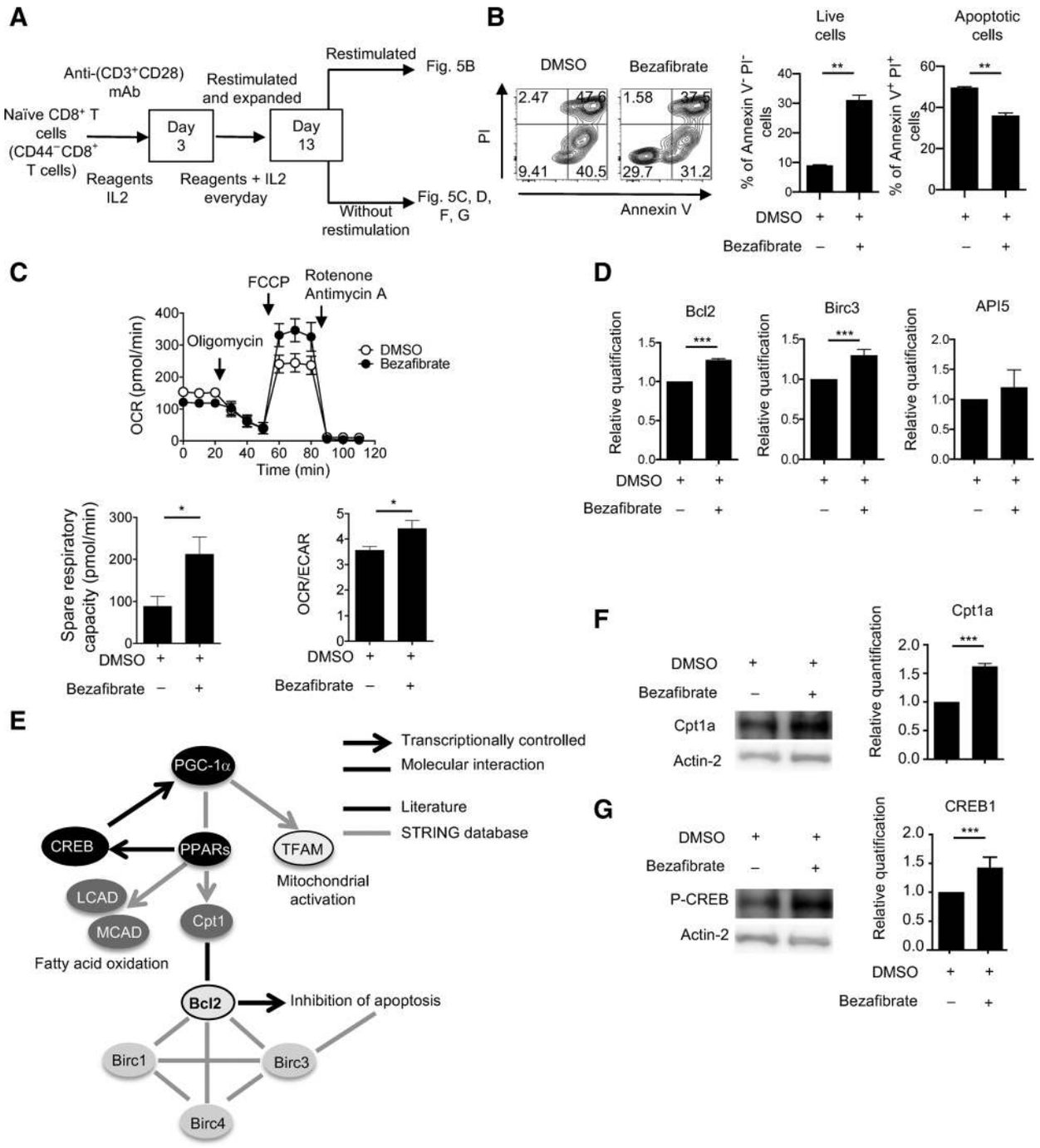

Figure 5.

Bezafibrate attenuates overactivation-induced apoptosis of CTLs *in vitro*. **A,** Naïve $CD8^+$ T cells ($CD44^-$ $CD8^+$ T cells) were isolated from the spleen of C57BL/6 mice and stimulated with anti-CD3 and anti-CD28 coated beads in presence of IL2 and bezafibrate on days 0 and 3. Cells were expanded in the presence of IL2 and bezafibrate until day 13 and used in the following experiments. **B,** T cells were restimulated on day 13 in the presence of bezafibrate for 24 hours. Annexin V and PI were used to stain live (annexin V^- PI^-) and apoptotic cells (annexin V^+ PI^+). Representative FACS profiles of annexin V and PI staining are given (left). Frequency of live and apoptotic cells was compared between treated groups. **C,** OCR of day 13 cells was measured by the Seahorse XF^e96 analyzer (left top). SRC were calculated (bottom left). OCR/ECAR ratio was measured (bottom right). **D,** *Bcl2*, *Birc3*, and *API5* expression was examined by quantitative PCR (qPCR) on day 13. **E,** Estimated downstream factors of the PGC-1α/PPAR axis including Bcl2, Cpt1a, and CREB are shown based on the STRING database and literature. **F–G,** Cpt1a (**F**) and pCREB (**G**) expression was determined by western blotting (left) and qPCR (right) using T cells on day 13. **B**, **D**, **F,** and **G,** Data represent the means ± SEM of 3 wells. Data are representative of two independent experiments. **, $P < 0.01$; ***, $P < 0.001$, two-tailed Student *t* test. **C,** Data represent the means ± SEM of 6 wells. *, $P < 0.05$, two-tailed Student *t* test.

Bezafibrate promotes proliferation of *in vitro*–stimulated naïve CD8$^+$ T cells

Our *in vivo* data suggest that enhanced proliferation of CTLs driven by the bezafibrate combination treatment contributes to increasing the number of effector killer T cells (Fig. 4E). To validate the effect of bezafibrate on T-cell proliferation, we stimulated naïve CD8$^+$ T cells with anti-CD3 and anti-CD28 in the presence of bezafibrate or solvent (DMSO) control. As shown in Fig. 6A, *in vitro*–stimulated naïve CD8$^+$ T cells in the presence of bezafibrate incorporated more ^{3}H-thymidine than those without bezafibrate. The enhancement of proliferation by bezafibrate treatment was confirmed by the dye dilution experiment (Supplementary Fig. S7A). Because bezafibrate treatment improved mitochondrial activities *in vivo*, we also investigated whether enhanced CTL proliferation *in vitro* by bezafibrate is accompanied by mitochondrial activation. As shown in Fig. 6B, both OCR and ECAR were significantly increased, indicating that CTL reached a higher energy state with bezafibrate treatment. Although ATP turnover and glycolytic capacity were upregulated, SRC was decreased in the bezafibrate-treated group (Fig. 6C). As bezafibrate treatment enhanced OCR values, we investigated its effect on other mitochondrial activation parameters. We found that bezafibrate-treated cells possess larger mitochondrial areas, higher intensity of MitoTrackerDeepRed, and more ROS than DMSO-treated cells, proving that mitochondria are activated during T-cell priming (Supplementary Fig. S7B). These data suggest that the effect of PPAR signaling on T-cell priming (day 2) is more associated with proliferation (anabolic pathway) than with longevity (catabolic pathway). Thus, PPAR signaling enhances proliferation during the early (priming) phase and inhibits apoptosis during the effector phase of the T cells.

Discussion

PD-1 blockade–based cancer immunotherapy has changed cancer treatment because it reaches more cancer targets and shows longer responses with fewer side effects than other cancer therapies (11, 33, 34). However, many patients do not respond to this therapy (12, 35). To enhance its efficacy and increase the range of patients who respond, combinatorial therapies involving PD-1 blockade have been designed and evaluated in clinical trials. One main cause of poor response is the absence or insufficiency of functional effector T cells at tumor sites, likely because of terminal differentiation and apoptosis mediated by PD-1 blockade (17, 27).

We found that bezafibrate treatment enhanced proliferation of CTLs and inhibited their apoptosis. Proliferation of primed CTLs generated more effector T cells. PPAR activation by bezafibrate enhanced both OCR and ECAR, explaining the upregulation of ATP production and glycolysis, both of which are necessary for induction of effector CTLs. These data are supported by studies showing that activation of both the mitochondria and PPAR/FAO pathways is necessary for proper activation of CTLs in the early stimulation phase (36, 37). The positive feed-forward loop in which PPAR signaling activates the mitochondria and enhances proliferation likely involves mTOR activation and promotes cellular proliferation through protein synthesis (38). mTOR signaling enhances cellular proliferation and AMPK activation improves cell survival (38). Therefore, the antiapoptotic and proproliferation effects of bezafibrate are indicated by our results showing that total CD8$^+$ T cells from DLN isolated from mice treated with anti–PD-L1 and a mitochondria-activating chemical showed upregulation of both AMPK and mTOR activity, even though mTOR and AMPK compete with each other with in a single cell (20, 38).

Chronological dissection of the effects of PD-1 blockade and bezafibrate is schematically represented (Supplementary Fig. S8). Upon activation, naïve T cells proliferate and acquire effector function, a process that requires energy generation by glycolysis (Supplementary Fig. S8A). To avoid terminal differentiation and cell death induced by overactivation, T cells express immune checkpoints such as PD-1 and shift their energy metabolic pathway to FAO/OXPHOS (19, 27, 39). The PD-1 signal confers T-cell longevity by compromising proliferation and killing activity, producing dysfunctional cells that may allow tumor cells to escape immune surveillance. In contrast, PD-1 blockade recovers T-cell effector function and reactivates effective antitumor immunity, which in turn promotes terminal differentiation and apoptosis accompanied by increased glycolysis and decreased FAO (Supplementary Fig. S8B; ref. 27). Thus, PD-1 blockade alone may reduce the number of functional effector T cells, which explain the incomplete responsiveness to PD-1 blockade. Introduction of pan-PPAR signaling in T cells by bezafibrate led to enhanced FAO, even in the PD-1 blocked state, and prolonged survival of CD8$^+$ T cells (Supplementary Fig. S8C). PPAR activation also boosts the proliferation of CD8$^+$ T cells, which increases the number of functional effector T cells (Supplementary Fig. S8C).

Our transcriptome analysis showed that PPAR pathway activation rescues PD-1 blockade–induced apoptosis in T cells by upregulating the antiapoptotic proteins Bcl2, Birc3, and API5. Gene-expression data revealed that the FAO pathway is promoted during PPAR stimulation, through increased expression of Cpt1, an enzyme key to fatty acid metabolism in mitochondria. Cpt1 is stabilized by interaction with Bcl2, and inhibition of Cpt1 enhances cell death (28). Our results suggest that PPAR inhibits apoptosis of CTLs by upregulating Bcl2, Cpt1, and cross-talk between PPAR and Bcl2 (29). The effect of the PPAR pathway on T-cell longevity is indicated by the improvement in mitochondrial SRC defined as the potential ATP levels in OXPHOS that can be used when energy demand surges. Thus, SRC enhancement in CTLs by bezafibrate suggests that CTLs can survive longer and increase their number in a memory-like pool (23). We observed more depolarized mitochondria (~55.2%) in the TIL under anti–PD-L1 plus bezafibrate therapy (Fig. 2F). This mitochondrial population characterized by low MitoTracker Deep Red and high MitoTracker Green supports longevity of T cells because cells with depolarized mitochondria would undergo mitophagy to eliminate damaged mitochondria and enhance cellular survival (40–42). Thus, bezafibrate treatment, which depolarizes mitochondria, would extend the life span of cells, as we observed.

PPAR signaling induces expression of a range of target genes (43). Our microarray data from CD8$^+$ T cells showed that many of the genes identified belong to energy metabolism-related pathways, e.g., *Cpt1*, *LCAD*, *MCAD*, hydroxyacyl-CoA dehydrogenase/3-ketoacyl-CoA thiolase/enoyl-CoA hydratase (trifunctional protein), β-subunit (*Hadhb*), malic enzyme 1 (*Me1*), Perillipin 2 (*Plin2*), and stearoyl-CoA desaturase-1 (*Scd1*). Our data also revealed additional genes induced by PPAR signaling. For instance, genes in pathways related to immune function were induced, including cytokine–cytokine receptor interactions, the

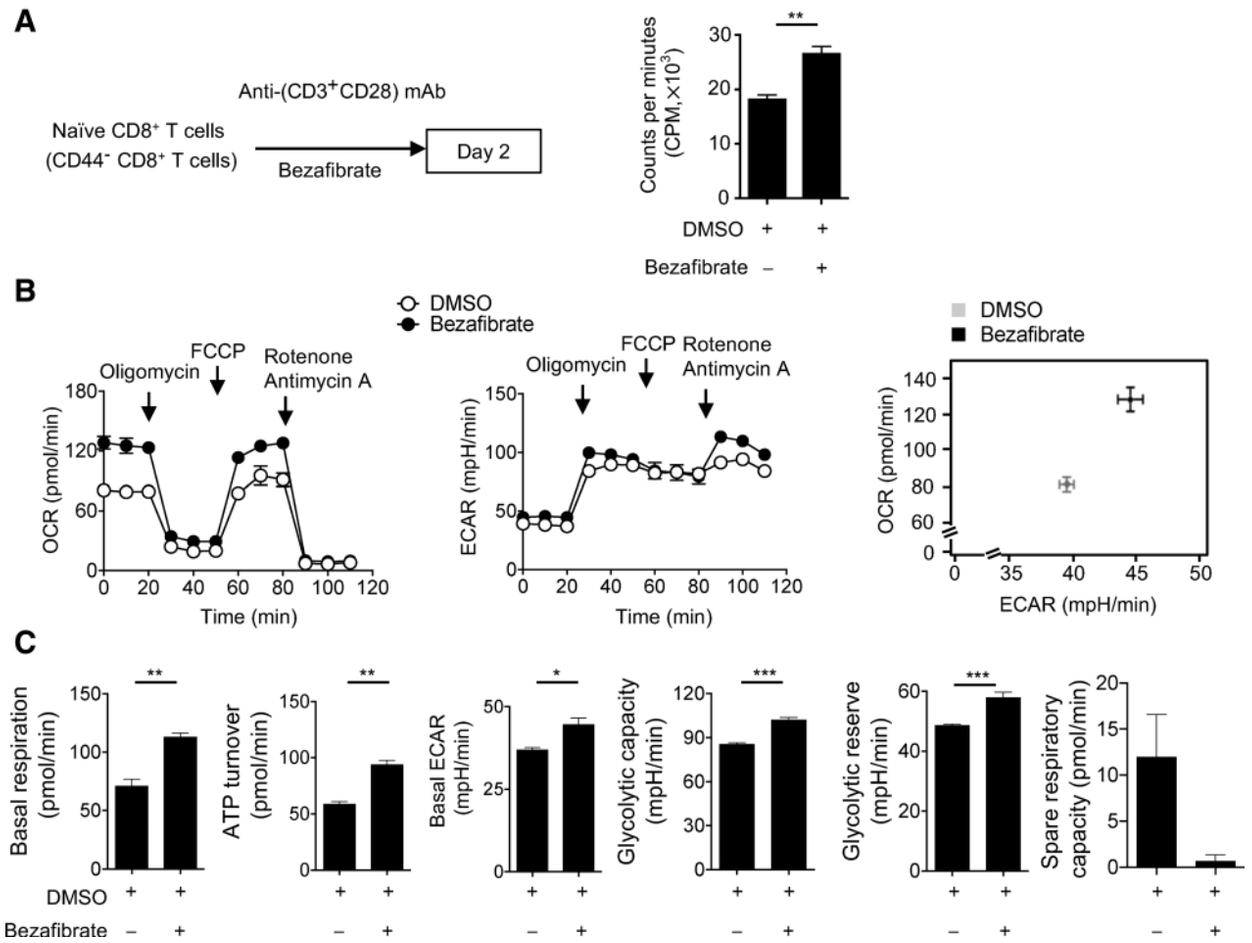

Figure 6.

Bezafibrate enhances proliferation of naïve CD8$^+$ T cells in the priming phase *in vitro*. **A,** Naïve CD8$^+$ T cells were isolated from the spleen of C57BL/6 mice, stimulated with anti-CD3 and anti-CD28–coated beads with bezafibrate for 2 days and used in the following experiments. T-cell proliferation was measured by ^{3}H-thymidine incorporation assays. Data represent the means ± SEM of 3 wells. **B,** OCR (left) and ECAR (middle) of day 2 cells were measured with the Seahorse XF^{e}96 analyzer. Basal OCR and ECAR values are plotted (right). **C,** Basal respiration, ATP turnover, basal ECAR, glycolytic capacity, glycolytic reserve, and SRC were calculated based on the data in **B**. **B** and **C,** Data represent the means ± SEM of 6 wells (**B** and **C**). Data are representative of two independent experiments. *, $P < 0.05$; **, $P < 0.01$; ***, $P < 0.001$, two-tailed Student *t* test.

chemokine signaling pathway, complement and coagulation cascades, and natural killer cell–mediated toxicity. Therefore, our data suggest additional mechanisms for regulating the killing activity of CD8$^+$ T cells by PPARs.

We found that each subset of the T-cell population (P1/P2/P3) exhibited different mitochondrial activities. However, the P3 population likely has a large contribution to the changes observed in the flux assay of total CD8$^+$ T cells for the following reasons. We demonstrated that, after bezafibrate treatment, mitochondrial activity was increased in the P3 population but not in others. Although naïve and memory populations (P1 and P2) are represented in T cells, mitochondrial activities do not change in these populations after the bezafibrate combination treatment. Further, the bezafibrate combination therapy increased the number of cells only in the P3 population. Therefore, it is likely that upregulation in the flux assay in the total CD8$^+$ T cells was mainly due to metabolic changes of the P3 population.

We previously showed that metabolic genes in tumor cells were unperturbed by treatment with Luperox or uncoupler alone (20). We expected that bezafibrate would not have large effect on tumor metabolism, as the dose used in this study was less than one-tenth the dose showing cytotoxicity toward tumor cells (44). If bezafibrate exerted its antiapoptotic effect or proproliferation effect on tumor cells, tumor growth would be faster compared with the untreated group. However, we observed no enhanced tumor growth *in vivo* when bezafibrate was administered alone, suggesting no direct effect of bezafibrate alone on tumor cells.

In summary, we showed that PPAR signaling reprograms CTL energy metabolism and overcomes the reduction in functional effector T-cell number associated with PD-1 blockade by decreasing apoptosis or increasing proliferation. Apoptosis was inhibited by upregulation of the antiapoptotic factor Bcl2 in CTLs. Enhanced proliferation can be explained by mitochondrial activation and upregulation of the mTOR pathway. Our

results will enable development of improved combination therapies and allow for the treatment of patients who are less responsive to therapy blocking the PD-1/PD-L1 interaction alone.

Disclosure of Potential Conflicts of Interest

No potential conflicts of interest were disclosed.

Authors' Contributions

Conception and design: P.S. Chowdhury, K. Chamoto, T. Honjo
Development of methodology: P.S. Chowdhury, K. Chamoto
Acquisition of data (provided animals, acquired and managed patients, provided facilities, etc.): P.S. Chowdhury, K. Chamoto, A. Kumar
Analysis and interpretation of data (e.g., statistical analysis, biostatistics, computational analysis): P.S. Chowdhury, K. Chamoto, A. Kumar
Writing, review, and/or revision of the manuscript: P.S. Chowdhury, K. Chamoto, T. Honjo
Study supervision: P.S. Chowdhury, A. Kumar, T. Honjo

Acknowledgments

This work was supported by AMED under grant numbers JP17cm0106302, JP17gm0710012 (T. Honjo), and JP171k1403006 (K. Chamoto); Tang Prize Foundation (T. Honjo); JSPS KAKENHI grant numbers JP16H06149, 17K19593 (K. Chamoto), and 17F17119 (P.S. Chowdhury); the Cell Science Foundation (K. Chamoto); and Takeda Science Foundation (A. Kumar).

We thank M. Al-Habsi, M. Akrami, T. Oura, R. Hatae, Y. Nakajima, R.M. Menzes, and K. Yurimoto for assistance in sample preparation; Y. Kitawaki for helping with the western blotting; N.A. Begum for helping with the GeneChip data analysis; and S. Fagarasan for many stimulating discussions. We thank Bristol-Myers Squibb for the collaboration.

The costs of publication of this article were defrayed in part by the payment of page charges. This article must therefore be hereby marked *advertisement* in accordance with 18 U.S.C. Section 1734 solely to indicate this fact.

Received February 16, 2018; revised May 16, 2018; accepted August 20, 2018; published first August 24, 2018.

References

1. Dunn GP, Old LJ, Schreiber RD. The immunobiology of cancer immunosurveillance and immunoediting. Immunity 2004;21:137–48.
2. Fife BT, Bluestone JA. Control of peripheral T-cell tolerance and autoimmunity via the CTLA-4 and PD-1 pathways. Immunol Rev 2008;224:166–82.
3. Poschke I, Mougiakakos D, Kiessling R. Camouflage and sabotage: tumor escape from the immune system. Cancer Immunol Immunother 2011;60:1161–71.
4. Leach DR, Krummel MF, Allison JP. Enhancement of antitumor immunity by CTLA-4 blockade. Science 1996;271:1734–6.
5. Iwai Y, Ishida M, Tanaka Y, Okazaki T, Honjo T, Minato N. Involvement of PD-L1 on tumor cells in the escape from host immune system and tumor immunotherapy by PD-L1 blockade. Proc Natl Acad Sci USA 2002;99:12293–7.
6. Phan GQ, Yang JC, Sherry RM, Hwu P, Topalian SL, Schwartzentruber DJ, et al. Cancer regression and autoimmunity induced by cytotoxic T lymphocyte-associated antigen 4 blockade in patients with metastatic melanoma. Proc Natl Acad Sci USA 2003;100:8372–7.
7. Brahmer JR, Drake CG, Wollner I, Powderly JD, Picus J, Sharfman WH, et al. Phase I study of single-agent anti-programmed death-1 (MDX-1106) in refractory solid tumors: safety, clinical activity, pharmacodynamics, and immunologic correlates. J Clin Oncol 2010;28:3167–75.
8. Hodi FS, O'Day SJ, McDermott DF, Weber RW, Sosman JA, Haanen JB, et al. Improved survival with ipilimumab in patients with metastatic melanoma. N Engl J Med 2010;363:711–23.
9. Topalian SL, Hodi FS, Brahmer JR, Gettinger SN, Smith DC, McDermott DF, et al. Safety, activity, and immune correlates of anti-PD-1 antibody in cancer. N Engl J Med 2012;366:2443–54.
10. Chowdhury PS, Chamoto K, Honjo T. Combination therapy strategies for improving PD-1 blockade efficacy: a new era in cancer immunotherapy. J Intern Med 2017.
11. Topalian SL, Drake CG, Pardoll DM. Immune checkpoint blockade: a common denominator approach to cancer therapy. Cancer Cell 2015;27:450–61.
12. Zou W, Wolchok JD, Chen L. PD-L1 (B7-H1) and PD-1 pathway blockade for cancer therapy: mechanisms, response biomarkers, and combinations. Sci Transl Med 2016;8:328rv4.
13. Boutros C, Tarhini A, Routier E, Lambotte O, Ladurie FL, Carbonnel F, et al. Safety profiles of anti-CTLA-4 and anti-PD-1 antibodies alone and in combination. Nat Rev Clin Oncol 2016;13:473–86.
14. Langer CJ, Gadgeel SM, Borghaei H, Papadimitrakopoulou VA, Patnaik A, Powell SF, et al. Carboplatin and pemetrexed with or without pembrolizumab for advanced, non-squamous non-small-cell lung cancer: a randomised, phase 2 cohort of the open-label KEYNOTE-021 study. Lancet Oncol 2016;17:1497–508.
15. Jass JR. Lymphocytic infiltration and survival in rectal cancer. J Clin Pathol 1986;39:585–9.
16. Taube JM, Anders RA, Young GD, Xu H, Sharma R, McMiller TL, et al. Colocalization of inflammatory response with B7-h1 expression in human melanocytic lesions supports an adaptive resistance mechanism of immune escape. Sci Transl Med 2012;4:127ra37.
17. Tumeh PC, Harview CL, Yearley JH, Shintaku IP, Taylor EJ, Robert L, et al. PD-1 blockade induces responses by inhibiting adaptive immune resistance. Nature 2014;515:568–71.
18. Buck MD, O'Sullivan D, Pearce EL. T cell metabolism drives immunity. J Exp Med 2015;212:1345–60.
19. Patsoukis N, Bardhan K, Chatterjee P, Sari D, Liu B, Bell LN, et al. PD-1 alters T-cell metabolic reprogramming by inhibiting glycolysis and promoting lipolysis and fatty acid oxidation. Nat Commun 2015;6:6692.
20. Chamoto K, Chowdhury PS, Kumar A, Sonomura K, Matsuda F, Fagarasan S, et al. Mitochondrial activation chemicals synergize with surface receptor PD-1 blockade for T cell-dependent antitumor activity. Proc Natl Acad Sci USA 2017;114:E761–E70.
21. Scharping NE, Menk AV, Moreci RS, Whetstone RD, Dadey RE, Watkins SC, et al. The tumor microenvironment represses T cell mitochondrial biogenesis to drive intratumoral T cell metabolic insufficiency and dysfunction. Immunity 2016;45:701–3.
22. Knox JJ, Cosma GL, Betts MR, McLane LM. Characterization of T-bet and eomes in peripheral human immune cells. Front Immunol 2014;5:217.
23. van der Windt GJ, Everts B, Chang CH, Curtis JD, Freitas TC, Amiel E, et al. Mitochondrial respiratory capacity is a critical regulator of CD8+ T cell memory development. Immunity 2012;36:68–78.
24. Tkachev V, Goodell S, Opipari AW, Hao LY, Franchi L, Glick GD, et al. Programmed death-1 controls T cell survival by regulating oxidative metabolism. J Immunol 2015;194:5789–800.
25. Picca A, Lezza AM. Regulation of mitochondrial biogenesis through TFAM-mitochondrial DNA interactions: Useful insights from aging and calorie restriction studies. Mitochondrion 2015;25:67–75.
26. Smith SA. Peroxisome proliferator-activated receptors and the regulation of mammalian lipid metabolism. Biochem Soc Trans 2002;30:1086–90.
27. Odorizzi PM, Pauken KE, Paley MA, Sharpe A, Wherry EJ. Genetic absence of PD-1 promotes accumulation of terminally differentiated exhausted CD8+ T cells. J Exp Med 2015;212:1125–37.
28. Paumen MB, Ishida Y, Han H, Muramatsu M, Eguchi Y, Tsujimoto Y, et al. Direct interaction of the mitochondrial membrane protein carnitine palmitoyltransferase I with Bcl-2. Biochem Biophys Res Commun 1997;231:523–5.
29. Perianayagam MC, Madias NE, Pereira BJ, Jaber BL. CREB transcription factor modulates Bcl2 transcription in response to C5a in HL-60-derived neutrophils. Eur J Clin Invest 2006;36:353–61.
30. Roy A, Jana M, Corbett GT, Ramaswamy S, Kordower JH, Gonzalez FJ, et al. Regulation of cyclic AMP response element binding and hippocampal plasticity-related genes by peroxisome proliferator-activated receptor alpha. Cell Rep 2013;4:724–37.

31. Handschin C, Rhee J, Lin J, Tarr PT, Spiegelman BM. An autoregulatory loop controls peroxisome proliferator-activated receptor gamma coactivator 1alpha expression in muscle. Proc Natl Acad Sci USA 2003;100:7111–6.
32. Fernandez-Marcos PJ, Auwerx J. Regulation of PGC-1alpha, a nodal regulator of mitochondrial biogenesis. Am J Clin Nutr 2011;93:884S–90.
33. Couzin-Frankel J. Breakthrough of the year 2013. Cancer immunotherapy. Science 2013;342:1432–3.
34. Okazaki T, Chikuma S, Iwai Y, Fagarasan S, Honjo T. A rheostat for immune responses: the unique properties of PD-1 and their advantages for clinical application. Nat Immunol 2013;14:1212–8.
35. Robert C, Long GV, Brady B, Dutriaux C, Maio M, Mortier L, et al. Nivolumab in previously untreated melanoma without BRAF mutation. N Engl J Med 2015;372:320–30.
36. Sena LA, Li S, Jairaman A, Prakriya M, Ezponda T, Hildeman DA, et al. Mitochondria are required for antigen-specific T cell activation through reactive oxygen species signaling. Immunity 2013;38:225–36.
37. Angela M, Endo Y, Asou HK, Yamamoto T, Tumes DJ, Tokuyama H, et al. Fatty acid metabolic reprogramming via mTOR-mediated inductions of PPARgamma directs early activation of T cells. Nat Commun 2016; 7:13683.
38. Chi H. Regulation and function of mTOR signalling in T cell fate decisions. Nat Rev Immunol 2012;12:325–38.
39. Zhang Y, Kurupati R, Liu L, Zhou XY, Zhang G, Hudaihed A, et al. Enhancing CD8(+) T cell fatty acid catabolism within a metabolically challenging tumor microenvironment increases the efficacy of melanoma immunotherapy. Cancer Cell 2017;32:377–91 e9.
40. Gomes LC, Scorrano L. Mitochondrial morphology in mitophagy and macroautophagy. Biochim Biophys Acta 2013;1833:205–12.
41. Narendra D, Tanaka A, Suen DF, Youle RJ. Parkin is recruited selectively to impaired mitochondria and promotes their autophagy. J Cell Biol 2008;183:795–803.
42. Zhu J, Wang KZ, Chu CT. After the banquet: mitochondrial biogenesis, mitophagy, and cell survival. Autophagy 2013;9:1663–76.
43. Lemay DG, Hwang DH. Genome-wide identification of peroxisome proliferator response elements using integrated computational genomics. J Lipid Res 2006;47:1583–7.
44. Panigrahy D, Kaipainen A, Huang S, Butterfield CE, Barnes CM, Fannon M, et al. PPARalpha agonist fenofibrate suppresses tumor growth through direct and indirect angiogenesis inhibition. Proc Natl Acad Sci USA 2008;105:985–90.